THE JOURNAL OF PHYSICAL CHEMISTRY C

Article

pubs.acs.org/JPCC

Plasma-Assisted Sulfur Doping of $LiMn_2O_4$ for High-Performance Lithium-Ion Batteries

Qianqian Jiang,[‡] Dongdong Liu,[†] Han Zhang,*[,‡] and Shuangyin Wang*[,†]

[†]State Key Laboratory of Chem/Bio-Sensing and Chemometrics, College of Chemistry and Chemical Engineering, Hunan University, 410082, Changsha, P. R. China

[‡]SZU-NUS Collaborative Innovation Center for Optoelectronic Science and Technology, Key Laboratory of Optoelectronic Devices and Systems of Ministry of Education and Guangdong Province, College of Optoelectronic Engineering, Shenzhen University, Shenzhen, 518060, P. R. China

Supporting Information

ABSTRACT: Though considered as one of the most promising materials for rechargeable Li-ion batteries, spinel $LiMn_2O_4$ suffers from fast capacity fading during cycling due to the structural instability, Jahn−Teller distortion, and Mn dissolution into the electrolyte. In order to improve the electrochemical performance, in this work, we, for the first time, realize the sulfur doping by the plasma-assisted method in $LiMn_2O_4$. Physical properties of the synthesized materials $LiMn_2O_{4-x}S_x$ are measured by XRD, SEM, and EDS, which confirm that S atoms have been successfully doped into the structure of $LiMn_2O_4$ ($LiMn_2O_{4-x}S_x$) with the high crystalline and uniform morphology. Compared to the pristine $LiMn_2O_4$ prepared by the conventional method (800 °C, 8 h), the $LiMn_2O_{4-x}S_x$ prepared by the plasma-assisted method shows superior performance with higher capacity (125.3 $mAh{\cdot}g^{-1}$) and significantly improved cycling stability (maintaining 97.76% of its initial discharge capacity after 60 cycles). In addition, the sulfur-doped $LiMn_2O_4$ demonstrates dramatically enhanced reversibility and stability even at the elevated temperature due to the improved structural stability and the suppressed Mn dissolution into the electrolyte by the doping of S. The sulfur doping into $LiMn_2O_4$ by the plasma-assisted method offers a new strategy for efficient modification of electrode materials for energy storage devices.

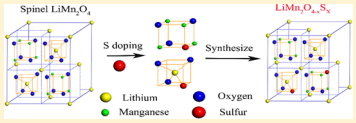

1. INTRODUCTION

Lithium secondary batteries (LIBs) with high energy density and power capability have succeeded in portable electronics such as cell phones and laptops.[1−3] Currently, $LiMn_2O_4$ is considered as one of the most promising materials with good electrochemical performance in lithium secondary batteries due to its low cost, environmental benign property, good thermal stability, high energy density, etc.[4−7] However, low practical capacity (≤120 $mAh{\cdot}g^{-1}$) and significant capacity loss of spinel $LiMn_2O_4$ during cycling prevent its wider use as the cathode material for lithium secondary batteries.[8−10] In addition, the serious capacity fading of $LiMn_2O_4$ at the temperature over 55 °C is another drawback.[11,12] The inferior capacity retention property at high temperature is caused by the Jahn−Teller effect and the Mn dissolution into the electrolyte.[13,14] The acidity of the electrolyte containing $LiPF_6$ at elevated temperature is attributed to the formation of HF acid due to the reaction of $LiPF_6$ with residual water in the electrolyte.[15] Therefore, the passivation LiF is produced by HF reacting with the cathode, which can accelerate the decline of cycling performance of the LIBs according to the following equation:[16,17]

$$2LiMn_2O_4 + 4H^+ \rightarrow 3\lambda\text{−}MnO_2(s) + Mn^{2+}(l) + 2Li^+(l) + 2H_2O \quad (1)$$

The modification of $LiMn_2O_4$ active material is considered to be essential to improve its performances. Hence, in order to solve the problems such as Mn dissolution and Jahn−Teller effect, the substitution of Mn with metal ions, by substituting a small fraction of the manganese ions with several metal ions (M = Al, Se, Mg, Zn, Co, Ti, Ni, Fe, Cr), has been attempted to stabilize the structure of $LiMn_2O_4$ during cycling,[18−21] which has been studied and considered as an effective way to enhance the cycling stability.

However, the electrochemical properties of cation-doped $LiMn_2O_4$ materials have not been improved at elevated temperature under repeated cycling conditions. According to the literature reports, the capacity loss of the $LiMn_2O_4$ electrode at high temperature can be minimized by replacing a small amount of the oxygen ion with other anions,[22,23] which indicates that the capacity of the spinel $LiMn_2O_4$ electrode could double, and the energy density of the lithium secondary batteries would increase by two-thirds if the Jahn−Teller distortion could be controlled. Anion doping on oxygen sites is effective in reducing impedance and lattice changes during cycling. Until now, there are very few reports about anion doping modification on spinel $LiMn_2O_4$.[24,25]

Herein, in the present study, we, for the first time, develop an efficient plasma strategy to realize the sulfur doping into $LiMn_2O_4$ to obtain oxysulfide $LiMn_2O_{4-x}S_x$ as the cathode materials of Li-ion batteries. The doped sulfur atoms would

Received: October 21, 2015
Revised: December 13, 2015
Published: December 14, 2015

DOI: 10.1021/acs.jpcc.5b10298
J. Phys. Chem. C 2015, 119, 28776−28782

occupy the oxygen site in $LiMn_2O_4$. The structure of the spinel-type $LiMn_2O_4$ and the possible structure $LiMn_2O_{4-x}S_x$ after S doping are shown in Scheme 1. It should be pointed out that

Scheme 1. Structures of Spinel-Type $LiMn_2O_4$ and $LiMn_2O_{4-x}S_x$

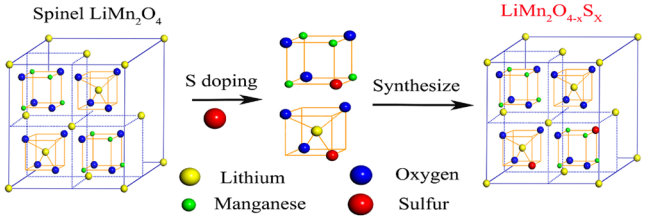

the plasma method is of high efficiency and low energy consumption. In plasma, the positive and negative ions are completely free, showing a high chemical activity. Therefore, the chemical reaction can be easily promoted. Structure and morphology of the cathode electrode after S doping ($LiMn_2O_{4-x}S_x$) are characterized by XPS, XRD, and SEM techniques, which preliminarily confirm S doping on the structure and the influence on the morphology. Cyclic voltammograms and electrochemical impedance spectroscopy are further used to analyze the effectiveness of S doping on the performance change of the $LiMn_2O_4$ electrode. The electrochemical performances of $LiMn_2O_{4-x}S_x$ are dramatically improved. Specially, the cycling performance at the elevated temperature is significantly enhanced.

2. EXPERIMENTAL SECTION

2.1. Material Preparation and Physical Characterization. The spinel $LiMn_2O_4$ was synthesized by the modified solid state method[26] using lithium hydroxide as a lithium source and MnO_2 as manganese sources as starting materials. The two reagents were mixed with a stoichiometric molar ratio of 1:2, and then ball-milled for 2 h. The mixture was calcined at 800 °C for 8 h to obtain $LiMn_2O_4$ (named as LMO-8h). The obtained $LiMn_2O_4$ and a measured amount of thiourea were grinded to make the uniform mixture. The molar ratio of $LiMn_2O_4$ and thiourea was 10:1. Then, the mixture was introduced into the plasma-coupled tube furnace. Plasma was generated by an RF power supply at 13.56 MHz, the temperature of the tube furnace was set at 300 °C, and the applied RF power was set at 200 W. The flow rate of argon was set at 2 sccm (standard-state cubic centimeter per minute), and the total pressure of the chamber was kept at about 60 Pa. The reaction time was adjusted from 10 to 30 min. The samples $LiMn_2O_{4-x}S_x$ synthesized by the above process were referred to as PLA-LMO-S-10, PLA-LMO-S-20, and PLA-LMO-S-30, respectively.

Powder X-ray diffraction (Rigaku, Rint-2000) using Cu Kα radiation was used to identify the crystalline phase of as-prepared powders, and the lattice parameters were determined by iterative least-squares refinements for the XRD patterns using the JADE program. The surface morphology and particle size of the powder were observed by scanning electron microscopy (SEM). XPS analysis was carried out on an ESCALAB 250Xi photoelectron spectrometer, and curve fitting and background subtraction were accomplished.

2.2. Cell Fabrication and Electrochemical Measurements. The different $LiMn_2O_4$ electrodes as-fabricated above were integrated into two-electrode CR2032-type coin cells for electrochemical measurements, where the $LiMn_2O_4$ electrode was used as working electrode with metallic lithium foil as counter and reference electrodes; the electrolyte consisted of 1.0 mol·L^{-1} $LiPF_6$ in ethylene carbonate (EC) and dimethyl carbonate (DMC) in a 1:1 (v/v) ratio. The galvanostatic charge/discharge measurement was performed on a LAND-CT2001A battery test system within the potential range of 3.0–4.5 V at 0.2 C using a LAND CT2001A battery tester (Wuhan, China) at room temperature. Cyclic voltammogram (CV) of the Li-ion coin cell was carried out by cyclic voltammetry on AUT85794 (made in the Netherland) between 3 and 4.5 V at a scan rate of 0.1 mV·s^{-1}. The electrochemical impedance spectroscopy (EIS) measurement was carried out on a frequency response analyzer (AUT85794, Netherlands) with the frequency range from 100 kHz to 10 mHz.

3. RESULTS AND DISCUSSION

The XRD patterns of LMO-8h and PLA-LMO-S are presented in Figure 1. The XRD patterns can be indexed to those

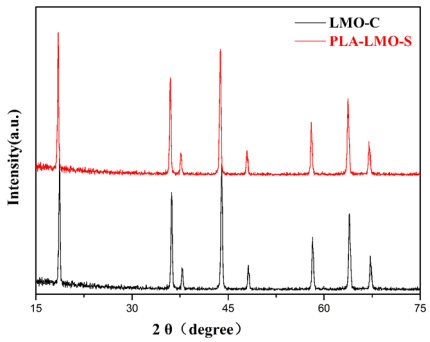

Figure 1. XRD patterns of LMO-8h and PLA-LMO-S.

reported in the JCPDS data (JCPDS No. 35-0782), which is also in good agreement with previous literatures,[27,28] thus demonstrating that the S-doped $LiMn_2O_4$ is successfully synthesized and the integral spinel structure of the material is reserved. Meanwhile, no other impurities peaks are found in the XRD pattern of PLA-LMO-S, meaning that the proper sulfur doping into $LiMn_2O_4$ has not generated any impurity in the final product. All the diffraction peaks of the two samples are indexed on the basis of a cubic structure with a space group of *Fd*3*m*, wherein the lithium ions (Li^+) occupied tetrahedral 8a sites and manganese ions (Mn^{5+} or Mn^{3+}), oxygen ions (O^{2-}), and sulfur ions (S^{2-}) resided in the octahedral 16d and the 32e sites,[29] which is consistent with the possible structure shown in Scheme 1. As seen in Table 1, the lattice constant (b) of the PLA-LMO-S is 8.203 Å, which is much lower than that of stoichiometric spinel (8.248 Å),[30] indicating that the lattice parameters decrease due to the introduction of sulfur by the plasma-assisted doping.

Table 1. Lattice Parameters of LMO-8h and PLA-LMO-S Obtained by Rietveld Refinement

	lattice parameters	
sample	a/Å	V/Å^3
JCPDS No. 35-0782	8.248	561.107
LMO-8h	8.239	559.273
PLA-LMO-S	8.203	551.973

DOI: 10.1021/acs.jpcc.5b10298
J. Phys. Chem. C 2015, 119, 28776–28782

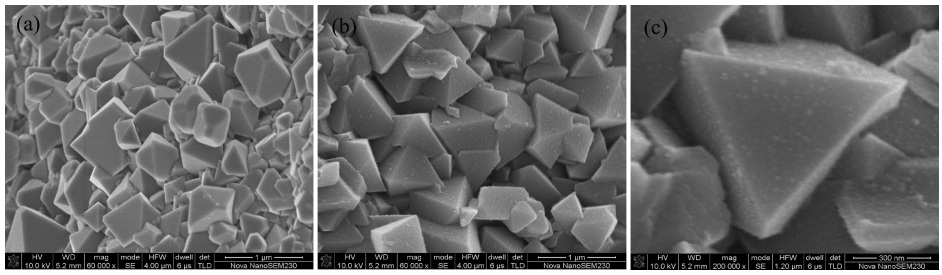

Figure 2. SEM images of LMO-8h (a) and PLA-LMO-S (b, c).

3.1. X-ray Photoelectron Spectroscopy, Electron Microscopy. In order to study the effect of S doping into $LiMn_2O_4$ on the change of surface morphology, the SEM images of the two samples are shown in Figure 2. From Figure 2a,b, we can see that the particle morphologies of the two samples are analogous to that of single-crystal-like gold with a cubic structure, which further indicates that the little amount of S doping does not destroy the structure of the spinel $LiMn_2O_4$. On the other hand, from Figure 2c, we can find that the surface of PLA-LMO-S is more rough than LMO-8h, which is possibly due to the plasma etching. Though the surface of PLA-LMO-S is relatively rough, it is very uniform, which may be beneficial to lithium insertion/deinsertion, as verified by the following electrochemical characterizations.

The EDS results of LMO-8h and PLA-LMO-S are shown in Figure S1. We can clearly see that the atomic number ratios of manganese and oxygen elements in the two samples are close to the 1:2, which are consistent with the atomic number ratio of manganese and oxygen in the molecular formula ($LiMn_2O_4$). In Figure S1a, no other elements except for Mn and O are detected from sample LMO-8h, which indicates that there is no impurity existing in the product. In contrast to Figure S1a, there is one more S element detected from sample PLA-LMO-S (Figure S1b), which validates that S has been doped into the $LiMn_2O_4$. It should be pointed out that the content of sulfur in the doped sample is relatively low, indicating that S atoms only replace a small part of O element in the sample.

XPS results can provide useful information on the composition and chemical states of different elements in materials to study the electronic structure of materials. As shown in Figure 3, the Mn 2p XPS spectra of LMO-8h and PLA-LMO-S are given. For the pristine sample (Figure 3a, LMO-8h), the XPS spectrum shows a $Mn_{2p3/2}$ feature at ~642.4 eV between the binding energies of Mn^{3+} (641.9 eV) and Mn^{4+} (643.2 eV), which is in good agreement with previous reports.[31,32] However, the Mn 2p XPS spectra of sample PLA-LMO-S (Figure 3b) shifts toward higher binding energies. Moreover, the deconvolution results show that the ratio of Mn (III) increases due to the higher oxidation state (Mn(IV) changing to Mn with a lower oxidation state (Mn (III)) after the S doping, which indicates that the S doping can possibly result in the lower Mn oxidation state. This result is consistent with the XRD data, suggesting the decrease in the lattice parameters after the S doping. In comparison, Mn 2p XPS spectra of PLA-LMO-S-20 are deconvoluted into four peaks, which has two peaks more than that of LMO-8h. The two peaks at 640.8 and 641.9 eV are corresponding to the Mn−S bond according to the XPS database SRD-20 of the National Institute of Standards and Technology (NIST). The appearance of this additional Mn−S peak, which is absent in the pristine sample (LMO-8h), is the indicator of Mn−S

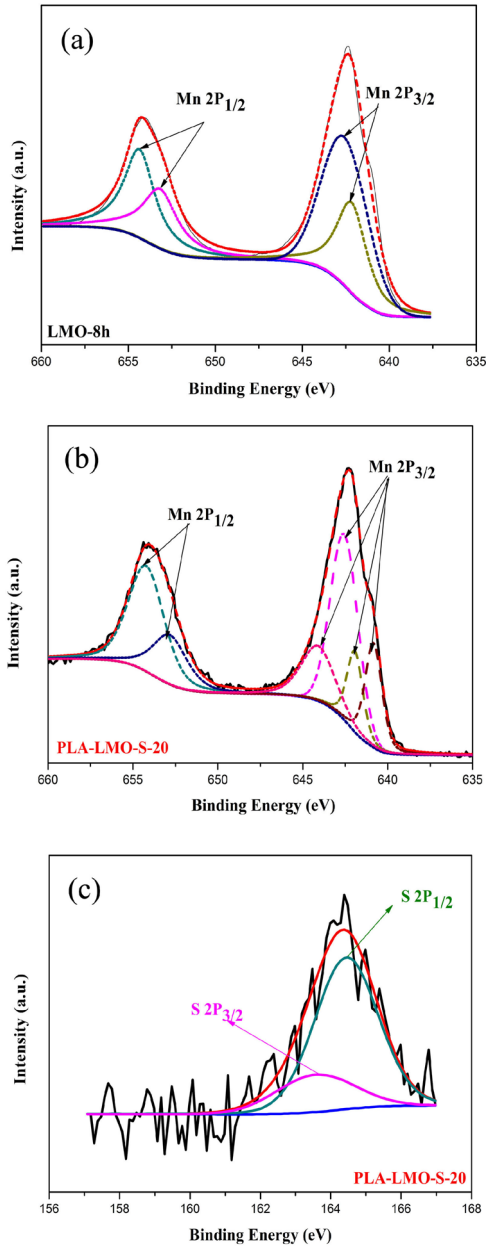

Figure 3. High-resolution Mn 2p XPS spectra of (a) LMO-8h and (b) PLA-LMO-S and (c) high-resolution S 2p XPS spectra of PLA-LMO-S.

interaction between Mn and S in the spinel structure, which is consistent with EDS results described above. From the S 2p XPS spectra of sample PLA-LMO-S in Figure 3c, we can see that $S_{2p3/2}$ and $S_{2p1/2}$ features exist in the sample, which can

DOI: 10.1021/acs.jpcc.5b10298
J. Phys. Chem. C 2015, 119, 28776−28782

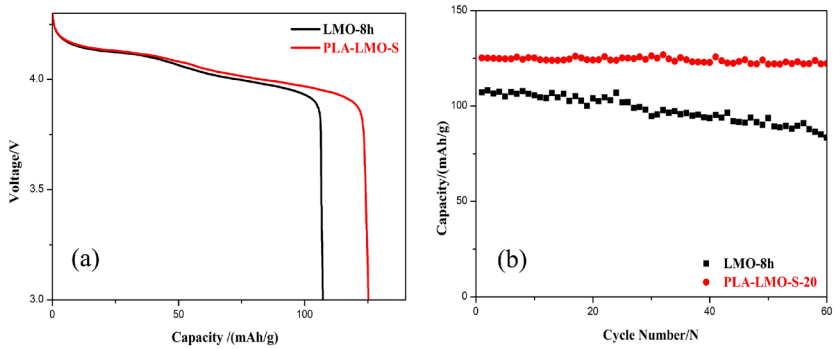

Figure 4. Discharge curves of LMO-8h and PLA-LMO-S in lithium-ion batteries at 0.2 C (a), and the corresponding cycling stability for 60 cycles (b).

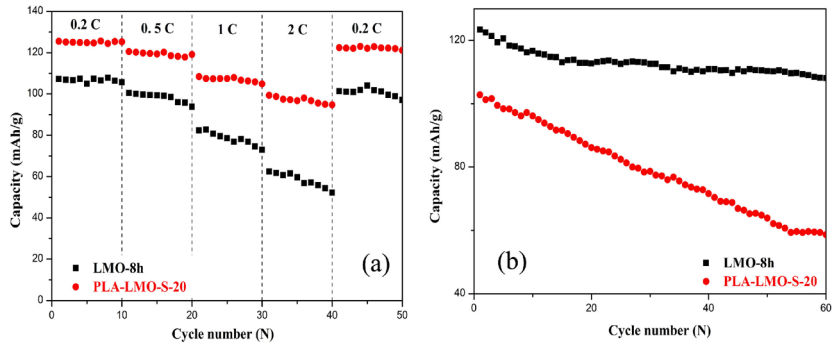

Figure 5. (a) Rate capabilities versus cycle number for the LMO-8h and PLA-LMO-S electrodes cycled at 0.2, 0.5, 1, 2, and 0.2 C rates between voltage limits of 3.0 and 4.3 V. (b) Cycling performance of the samples LMO-8h and PLA-LMO-S at 55 °C at the rate of 0.1 C in the voltage range of 3.0−4.5 V.

further confirm that the doped S has partially substituted the O sites to form the new bond Mn−S, which can make the spinel structure more stable.

3.2. Electrochemical Characterization. Since the sulfur doping does not seriously alter the spinel structure of $LiMn_2O_4$, the as-obtained sulfur-doped $LiMn_2O_4$ could act as the cathode materials in lithium-ion batteries. In the meantime, the modified electronic and structural properties of $LiMn_2O_4$ by the proper S doping may be beneficial for the battery performance. The electrochemical performance of the sulfur-doped cathodes was subsequently investigated by comparison with the conventional cathode without doping. Figure 4a shows the initial discharge capacity of materials LMO-8h and PLA-LMO-S at 0.2 C in the voltage range of 3−4.3 V at room temperature. The initial discharge curves of the two samples exhibit two voltage plateaus between 3 and 4.3 V, which indicates that the insertion and extraction of lithium ions occur in two stages.[33] The initial discharge capacity of PLA-LMO-S (125.2 $mAh{\cdot}g^{-1}$) is much higher than that of LMO-8h (107.2 $mAh{\cdot}g^{-1}$). At the same time, the initial discharge capacities of the doped cathode with different plasma times are also higher than that of LMO-8h, as given in Figure S2a, confirming the important role of the doped sulfur atoms. It is well-known that the typical discharge curve of the $LiMn_2O_4$ electrode usually has the S-shaped low-voltage region (3−4.15 V) and the L-shaped high-voltage region (4.15−4.3 V).[14] However, the discharge platform of PLA-LMO-S is longer than that of LMO-8h, which implies a better electrochemical performance contributed by the sulfur doping. The higher discharge capacity suggests that a small amount of substitution of S for O is very effective in prohibiting the formation of a tetragonal $Li_2Mn_2O_4$ structure on the $LiMn_2O_4$ host at the lower voltage range, which can make the material possess better performance. In previous reports, the decrease of initial discharge capacity was also observed in metal-doped $LiMn_2O_4$ because of the reduction of dissolved Mn.[30,34]

Cycling performance is another important electrochemical characteristic of lithium secondary batteries. Sulfur doping may affect the cycling performance of the sample by improving its structural stability. A comparison of the cycling behaviors of LMO-8h and PLA-LMO-S is explored to investigate their electrochemical stabilities. The cycling stability for the samples between 3.0 and 4.5 V at 0.2 C is shown in Figure 4b. The discharge capacities of PLA-LMO-S only decreased from 125.2 to 122.4 $mAh{\cdot}g^{-1}$ after 60 cycles with an average capacity loss of 0.046 $mAh{\cdot}g^{-1}$ per cycle, whereas the discharge capacity of LMO-4h decreases seriously from 107.2 to 83.5 $mAh{\cdot}g^{-1}$ after 60 cycles. It is obvious that PLA-LMO-S shows better cycling performance with the retention of 97.76% after 60 cycles, but the sample LMO-8h only shows the retention of 83.5%. The excellent cycling performance of PLA-LMO-S could be possibly attributed to the S doping into the spinel $LiMn_2O_4$, which can prohibit Mn ion distorting from cubic phase to tetragonal phase in $LiMn_2O_4$ and dissolving into the electrolyte. At the same time, the Jahn−Teller distortion is also restrained. In order to further confirm the effect on the cycling performance of S doping, the samples with different plasma times are investigated in Figure S2b. The capacity retentions of samples PLA-LMO-S-10, PLA-LMO-S-20, and PLA-LMO-S-30 are 80.48, 97.76, and 87.09%, respectively, which indicates that the sample PLA-LMO-S-20 has the best electrochemical performance among the three samples, which is closely related to their structural

DOI: 10.1021/acs.jpcc.5b10298
J. Phys. Chem. C 2015, 119, 28776−28782

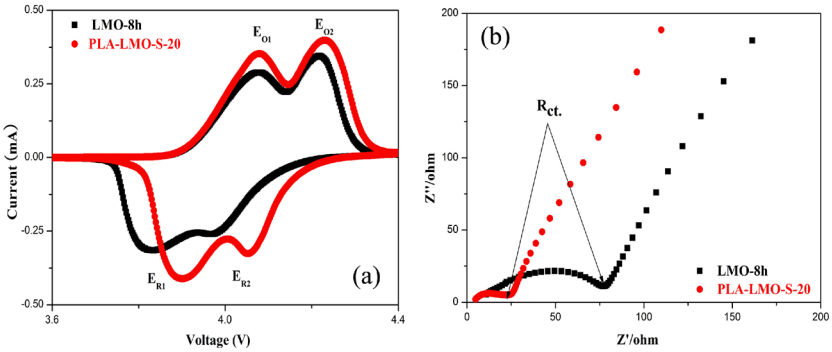

Figure 6. (a) Cyclic voltammogram curves at a scan rate of 0.1 mV/s and (b) electrochemical impedance spectra of the batteries with LMO-8h and PLA-LMO-S as the cathodes.

characteristics, that is, smaller unit cell volume and higher crystallinity. These results clearly indicate that the S doping plays an important role in improving the cycling performance of the spinel $LiMn_2O_4$, which can be used as a promising method to improve the electrochemical performance of the cathode material in lithium-ion batteries.

Rate capability is one of the important electrochemical characteristics of lithium secondary batteries. The rate capabilities of LMO-8h and PLA-LMO-S during cycling at different rates, varying from 0.2 to 2 C, are represented in Figure 5a. The first specific discharge capacities of LMO-8h and PLA-LMO-S are 105.7 and 125.3 mAh·g^{-1} at 0.2 C after 10 cycles. Compared with the low rate, the specific capacities of LMO-8h are 93.8, 72.9, and 52.2 mAh·g^{-1}, and their capacity retentions after 10 cycles are 93.33, 88.47, and 83.65% at 0.5, 1, and 2 C, respectively. The PLA-LMO-S shows a faster increase in capacity than pure $LiMn_2O_4$, and the reversible capacities of sample PLA-LMO-S-20 are 119.2, 104.9, and 94.8 mAh·g^{-1}, at 0.5, 1, and 2C after 10 cycles, corresponding to 1.16, 3.23, and 4.63% capacity fading, respectively. The results are apparently much better than the rate performance of the other modified $LiMn_2O_4$ reported in the literature.[34] The rate performance of PLA-LMO-S at the current density range between 0.2 and 2 C is obviously better than that of LMO-8h, which indicates that Li-ion insertion/extraction into/out of the $LiMn_2O_4$ lattice structure is kinetically improved by the doping of S. At the same time, the bond energy between Mn and S is bigger than that of Mn and O, which can make the whole structure more stable. Therefore, Jahn−Teller distortion and Mn dissolution into the electrolyte can be possibly reduced to a certain extent. Because of the stable structure of the PLA-LMO-S, Li^+ insertion/extraction can easily proceed, which is good for the rate performance of the cathode material. It indicates that the S doping can effectively elevate the cycling performances of the material. It will be further confirmed and supported by the cycling performances at the elevated temperature.

Even though $LiMn_2O_4$ is considered as one of the most promising cathode materials for lithium-ion batteries, the poor performance of $LiMn_2O_4$ at elevated temperature has been one of the major problems which hinders its further commercial application. Figure 5b presents the cycling performance of LMO-8h and PLA-LMO-S at 55 °C at the rate of 0.1 C, and it clearly demonstrates that the S doping can significantly reduce the capacity fade of $LiMn_2O_4$ under the elevated-temperature conditions. In contrast, the LMO-8h exhibits a discharge capacity declining from 102.8 to 58.6 mAh·g^{-1}, with a serious capacity loss of 43.0% after 60 cycles. However, the PLA-LMO-S maintains 87.60% of its initial capacity; in other words, it exhibits a slow capacity fading on cycling with an average capacity loss of 0.255 mAh·g^{-1} per cycle during 60 charge−discharge cycles. From the result of the elevated-temperature performance, we can clearly see that the S doping can significantly enhance the elevated-temperature durability of the cathode in lithium-ion batteries, probably due to the suppression of the dissolution of Mn species from the $LiMn_2O_4$ lattice to the electrolyte. The excellent elevated-temperature property of PLA-LMO-S is consistent with the other electrochemical performance tests, which further indicates that the S doping plays a vital role in improving the electrochemical performance of the cathode material. This finding clearly demonstrates that the S-doped $LiMn_2O_4$ ($LiMn_2O_{4-x}S_x$) synthesized by the novel plasma-assisted method has the excellent electrochemical performance for lithium-ion batteries.

The cyclic voltammograms (CV) of LMO-8h and PLA-LMO-S are presented in Figure 6a with the potential range between 3.6 and 4.4 V versus Li/Li^+ at a sweep rate of 0.1 mV/s at room temperature. It clearly shows that there are two couples of redox peaks on each cyclic voltammogram at around 3.9 and 4.1 V, which is consistent with initial discharge results shown in Figure 4a. The CV curves of two electrodes show two pairs of peaks corresponding to a two-step reversible intercalation reaction, in which lithium ions occupy two different tetragonal 8a sites in spinel $Li_xMn_2O_4$ ($x < 1$).[35] It further confirms that two kinds of reversible electrochemical reactions are involved in $LiMn_2O_{4-x}S_x$ during cycling. These two pairs of redox peaks reflect the typical oxidation processes of $LiMn_2O_4$ in 4.05 and 4.15 V (versus Li/Li^+) and deoxidation processes in the 3.95 and 4.05 V, which involves phase transitions.[36] The corresponding data obtained from Figure 6a are listed in Table S1 in detail. Two couples of separate redox peaks (the anodic peak E_{O1} and E_{O2}, the cathodic peak E_{R1} and E_{R2}) are observed from CV curves of LMO-8h and PLA-LMO-S. The split of redox peaks into two couples corresponds to two steps of the deintercalation and intercalation of Li^+ ions from/into the spinel host structure in the electrolyte.[37] Meanwhile, in comparison with the CV curve of sample LMO-8h, the PLA-LMO-S shows higher oxidation peak current density at higher potential, and higher reduction peak current density at lower potential with a relatively larger integrated area. This result indicates that this sample has the lower polarization and better reversible oxidation reaction process at the cathode, which further illustrates that S doping into the structure of spinel $LiMn_2O_4$ can effectively improve the electronic conductivity,

DOI: 10.1021/acs.jpcc.5b10298
J. Phys. Chem. C 2015, 119, 28776−28782

which is better than that of undoped spinel $LiMn_2O_4$. Furthermore, redox peaks of PLA-LMO-S are sharper than those of LMO-8h, indicating that PLA-LMO-S has larger capacity and faster electrode reaction than LMO-8h. In addition, the peak potential difference (depicted as $\Delta E1$ and $\Delta E2$ in Table S1) between each oxidation−reduction reaction is reduced by the S doping, which is a better explanation that the electrode potential of Li^+ insertion/extraction reactions in $LiMn_2O_{4-x}S_x$ is much closer to the equilibrium redox potential compared with that of LMO-8h. Therefore, this cyclic voltammetric behavior further confirms that PLA-LMO-S has the higher initial discharge capacity and better cycling performance, indicating that S doping plays a vital role in improving the electrochemical performance of cathode material.

Electrochemical impedance spectroscopy (EIS) is another useful tool to identify the kinetics of lithium intercalation/deintercalation into electrodes.[38] In order to get insight into the interaction of active material and the electrodes, electrochemical impedance spectroscopy before charge/discharge test with the two-electrode CR2032-type coin cells is carried out. Generally, an intercept at the Z_{real} axis in the high frequency region corresponds to the Ohmic resistance (R_s).[39] The second semicircle in the middle frequency range indicates the charge transfer resistance (R_{ct}).[40] The inclined line in the lower frequency represents the Warburg impedance (Z_W),[41] which is associated with lithium-ion diffusion in the $LiMn_2O_4$ particles. As shown in Figure 6b, the Ohmic resistances of LMO-8h and PLA-LMO-S have no marked difference, but the charge transfer resistance of LMO-8h is much bigger than that of PLA-LMO-S. EIS plots are fitted using the equivalent circuit model. From the fitted impedance parameters, the charge transfer resistance (R_{ct}) of the sample PLA-LMO-S is much smaller ($R_{ct} \approx 16.3$ Ω) than that of LMO-8h ($R_{ct} \approx 90.1$ Ω), indicating that the inserting and deinserting of lithium ions for PLA-LMO-S are easier than those for LMO-8h. Because the charge transfer is related to the interparticle contact, which depends on the physical structure of electrode materials, the EIS experiments also show that the pristine LMO-8h has a rapid decrease in the charge transfer resistance after S doping, which further suggests that the doping of sulfur atoms can make the spinel structure more stable, resulting in suppressed manganese dissolution and Jahn−Teller effect. The increased Li-ion migration resistance and high cell polarization of LMO-8h lead to an incomplete charging, which is bad for the electrochemical performance of cathode material. That means the PLA-LMO-S synthesized by the novel plasma-assisted process can enhance the Li^+ transportation, leading to much improved high rate capability and elevated-temperature performance.

4. CONCLUSIONS

In summary, the $LiMn_2O_{4-x}S_x$ as cathode materials of rechargeable Li-ion batteries has been successfully synthesized by the highly efficient plasma-assisted method. The structural and morphological analysis reveals that the $LiMn_2O_{4-x}S_x$ has the similar cubic spinel structure with the pristine $LiMn_2O_4$, but it has better crystallinity and uniform morphology than the pristine one. The XPS spectra not only confirm the difference of chemical valence of Mn element between the two samples but also further illustrate that the S partially substituted the O sites to form the new bond Mn−S. Compared to the pristine $LiMn_2O_4$, the synthesized $LiMn_2O_{4-x}S_x$ reveals higher specific discharge capacity, and better rate capability contributed by the S doping into the structure of $LiMn_2O_4$. Moreover, it demonstrates enhanced electrochemical properties with respect to the pristine $LiMn_2O_4$ at the elevated temperature, because of the suppression of Mn dissolution and the reduction of electrode resistance after the S doping. Therefore, the $LiMn_2O_{4-x}S_x$ prepared by doping S into the structure of $LiMn_2O_4$ by the novel plasma-assisted method is one of the most promising candidate materials for lithium-ion batteries.

■ ASSOCIATED CONTENT

Supporting Information

The Supporting Information is available free of charge on the ACS Publications website at DOI: 10.1021/acs.jpcc.5b10298.

EDS of the samples, electrochemical parameters, electrochemistry data of tested electrodes, and peak positions obtained from the cyclic voltammograms of samples (PDF)

■ AUTHOR INFORMATION

Corresponding Authors

*E-mail: shuangyinwang@hnu.edu.cn. Tel: +8618575520589 (S.W.).

*E-mail: hzhang@szu.edu.cn. Tel: +8615717490106 (H.Z.).

Notes

The authors declare no competing financial interest.

■ ACKNOWLEDGMENTS

The work is supported by the National Natural Science Foundation of China (Grant Nos. 51402100, 21573066, and 61435010), the Youth 1000 Talent Program of China, and the Interdiscipline Research Program of Hunan University.

■ REFERENCES

(1) Xu, K. Nonaqueous Liquid Electrolytes for Lithium-Based Rechargeable Batteries. *Chem. Rev.* **2004**, *104*, 4303−4417.

(2) Scrosati, B. Battery Technology-Challenge of Portable Power. *Nature* **1995**, *373*, 557−558.

(3) Armand, M.; Tarascon, J. M. Building Better Batteries. *Nature* **2008**, *451*, 652−657.

(4) Song, D.; Ikuta, H.; Uchida, T.; Wakihara, M. The Spinel Phases $LiAl_yMn_{2-y}O_4$ (Y = 0, 1/12, 1/9, 1/6, 1/3) and $Li(Al, M)_{1/6}Mn_{11/6}O_4$(M = Cr, Co) as the Cathode for Rechargeable Lithium Batteries. *Solid State Ionics* **1999**, *117*, 151−156.

(5) Tarascon, J.; Wang, E.; Shokoohi, F.; Mckinnon, W.; Colson, S. In The Spinel Phase of $LiMn_2O_4$ as a Cathode in Secondary Lithium Cells. *J. Electrochem. Soc.* **1991**, *138*, 2859−2864.

(6) Thackeray, M. M.; David, W. I. F.; Bruce, P. G.; Goodenough, J. B. Lithium Insertion into Manganese Spinels. *Mater. Res. Bull.* **1983**, *18*, 461−472.

(7) Jiang, Q.; Xu, L.; Ma, Z.; Zhang, H. Carbon Coated to Improve the Electrochemical Properties of $LiMn_2O_4$ Cathode Material Synthesized by the Novel Acetone Hydrothermal Method. *Appl. Phys. A: Mater. Sci. Process.* **2015**, *119*, 1069−1074.

(8) Thackeray, M. M. Manganese Oxides for Lithium Batteries. *Prog. Solid State Chem.* **1997**, *25*, 1−71.

(9) Jang, D. H.; Shin, Y. J.; Oh, S. M. Dissolution of Spinel Oxides and Capacity Losses in 4v $Li/Li_xMn_2O_4$ Coils. *J. Electrochem. Soc.* **1996**, *143*, 2204−2211.

(10) Jiang, H.; Fu, Y.; Hu, Y.; Yan, C.; Zhang, L.; Lee, P. S.; Li, C. Hollow $LiMn_2O_4$ Nanocones as Superior Cathode Materials for Lithium-Ion Batteries with Enhanced Power and Cycle Performances. *Small* **2014**, *10*, 1096−1100.

(11) Shim, J.; Kostecki, R.; Richardson, T.; Song, X.; Striebel, K. A. Electrochemical Analysis for Cycle Performance and Capacity Fading

DOI: 10.1021/acs.jpcc.5b10298
J. Phys. Chem. C 2015, 119, 28776−28782

of a Lithium-Ion Battery Cycled at Elevated Temperature. *J. Power Sources* **2002**, *112*, 222−230.
(12) Rodríguez-Carvajal, J.; Rousse, G.; Masquelier, C.; Hervieu, M. Electronic Crystallization in a Lithium Battery Material: Columnar Ordering of Electrons and Holes in the Spinel $LiMn_2O_4$. *Phys. Rev. Lett.* **1998**, *81*, 4660−4663.
(13) Xia, Y.; Zhou, Y.; Yoshio, M. Capacity Fading on Cycling of 4 V $Li/LiMn_2O_4$ Cells. *J. Electrochem. Soc.* **1997**, *144*, 2593−2600.
(14) Goodenough, J. B. Cathode Materials: A Personal Perspective. *J. Power Sources* **2007**, *174*, 996−1000.
(15) Myung, S. T.; Komaba, S.; Hirosaki, N.; Kumagai, N. Preparation of Layered $LiMn_xCr_{1-x}O_2$ Solid Solution by Emulsion Drying Method as Lithium Intercalation Compounds. *Electrochem. Commun.* **2002**, *4*, 397−401.
(16) Komaba, S.; Kumagai, N.; Sasaki, T.; Miki, Y. Manganese Dissolution from Lithium Doped Li-Mn-O Spinel Cathode Materials into Electrolyte Solution. *Electrochemistry* **2001**, *69*, 784−787.
(17) Alcantara, R.; Jaraba, M.; Lavela, P.; Tirado, J. L. New $LiNi_yCo_{1-2y}Mn_{1+y}O_4$ Spinel Oxide Solid Solutions as 5 V Electrode Material for Li-Ion Batteries. *J. Electrochem. Soc.* **2004**, *151*, A53−A58.
(18) Julien, C.; Ziolkiewicz, S.; Lemal, M.; Massot, M. Synthesis, Structure and Electrochemistry of $LiMn_{2-y}Al_yO_4$ Prepared by a Wet-Chemistry Method. *J. Mater. Chem.* **2001**, *11*, 1837−1842.
(19) Deng, B.; Nakamura, H.; Zhang, Q.; Yoshio, M.; Xia, Y. Greatly Improved Elevated-Temperature Cycling Behavior of $Li_{1+x}Mg_yMn_{2-x-y}O_{4+\delta}$ Spinels with Controlled Oxygen Stoichiometry. *Electrochim. Acta* **2004**, *49*, 1823−1830.
(20) Kim, G.-H.; Kim, J.-H.; Myung, S.-T.; Yoon, C. S.; Sun, Y.-K. Improvement of High-Voltage Cycling Behavior of Surface-Modified $LiNi_{1/3}Co_{1/3}Mn_{1/3}O_2$ Cathodes by Fluorine Substitution for Li-Ion Batteries. *J. Electrochem. Soc.* **2005**, *152*, A1707−A1713.
(21) Fu, Y.; Jiang, H.; Hu, Y.; Dai, Y.; Zhang, L.; Li, C. Synergistic Enhancement Effect of Al Doping and Highly Active Facets of $LiMn_2O_4$ Cathode Materials for Lithium-Ion Batteries. *Ind. Eng. Chem. Res.* **2015**, *54*, 3800−3805.
(22) Kim, G.-H.; Kim, M.-H.; Myung, S.-T.; Sun, Y. K. Effect of Fluorine on $Li[Ni_{1/3}Co_{1/3}Mn_{1/3}]O_{2-z}F_z$ as Lithium Intercalation Material. *J. Power Sources* **2005**, *146*, 602−605.
(23) Kubo, K.; Fujiwara, M.; Yamada, S.; Arai, S.; Kanda, M. Synthesis and Electrochemical Properties for $LiNiO_2$ Substituted by Other Elements. *J. Power Sources* **1997**, *68*, 553−557.
(24) Chan, H. W.; Duh, J. G.; Sheen, S. R. $LiMn_2O_4$ Cathode Doped with Excess Lithium and Synthesized by Co-Precipitation for Li-Ion Batteries. *J. Power Sources* **2003**, *115*, 110−118.
(25) Xia, Y.; Sakai, T.; Fujieda, T.; Yang, X. Q.; Sun, X.; Ma, Z. F.; McBreen, J.; Yoshio, M. Correlating Capacity Fading and Structural Changes in $Li_{1+y}Mn_{2-y}O_{4-\delta}$Spinel Cathode Materials: A Systematic Study on the Effects of Li/Mn Ratio and Oxygen Deficiency. *J. Electrochem. Soc.* **2001**, *148*, A723−A729.
(26) Jiang, Q.; Wang, X.; Miao, C.; Tang, Z. Synthesis and Characterization of Spinel $LiMn_2O_4$ Prepared by the Cyclohexanone Hydrothermal Method. *RSC Adv.* **2013**, *3*, 12088−12090.
(27) Chen, Y.; Xie, K.; Pan, Y.; Zheng, C. Nano-Sized $LiMn_2O_4$ Spinel Cathode Materials Exhibiting High Rate Discharge Capability for Lithium-Ion Batteries. *J. Power Sources* **2011**, *196*, 6493−6497.
(28) Sun, Y.-K.; Oh, B.; Lee, H. J. Synthesis and Electrochemical Characterization of Oxysulfide Spinel $LiAl_{0.15}Mn_{1.85}O_{3.97}S_{0.03}$ Cathode Materials for Rechargeable Batteries. *Electrochim. Acta* **2000**, *46*, 541−546.
(29) Ramana, C. V.; Massot, M.; Julien, C. M. Xps and Raman Spectroscopic Characterization of $LiMn_2O_4$ Spinels. *Surf. Interface Anal.* **2005**, *37*, 412−416.
(30) Shaju, K. M.; Subba Rao, G. V.; Chowdari, B. V. R. Lithiated O_2 Phase, $Li_{(2/3)+x}(Co_{0.15}Mn_{0.85})O_2$ as Cathode for Li-Ion Batteries. *Solid State Ionics* **2002**, *152*−*153*, 69−81.
(31) Xia, Y.; Yoshio, M. An Investigation of Lithium Ion Insertion into Spinel Structure Li-Mn-O Compounds. *J. Electrochem. Soc.* **1996**, *143*, 825−833.
(32) Han, D. W.; Ryu, W. H.; Kim, W. K.; Eom, J. Y.; Kwon, H. S. Effects of Li and Cl Codoping on the Electrochemical Performance and Structural Stability of $LiMn_2O_4$ Cathode Materials for Hybrid Electric Vehicle Applications. *J. Phys. Chem. C* **2013**, *117*, 4913−4919.
(33) Miura, K.; Yamada, A.; Tanaka, M. Electric States of Spinel $Li_xMn_2O_4$ as a Cathode of the Rechargeable Battery. *Electrochim. Acta* **1996**, *41*, 249−256.
(34) Xia, Y.; Yoshio, M. Studies on Li-Mn-O Spinel System (Obtained from Melt-Impregnation Method) as a Cathode for 4 V Lithium Batteries Part Iv. High and Low Temperature Performance of $LiMn_2O_4$. *J. Power Sources* **1997**, *66*, 129−133.
(35) Kim, M. G.; Kim, H.; Cho, J. V_2O_5-Coated TiO_2 Nanorod Electrodes. *J. Electrochem. Soc.* **2010**, *157*, A802−A807.
(36) Shaju, K. M.; Subba Rao, G. V.; Chowdari, B. V. R. Influence of Li-Ion Kinetics in the Cathodic Performance of Layered $Li(Ni_{1/3}Co_{1/3}Mn_{1/3})O_2$. *J. Electrochem. Soc.* **2003**, *151*, A1324−A1332.
(37) Levi, M. D.; Salitra, G.; Markovsky, B.; Teller, H.; Aurbach, D.; Heider, U.; Heider, L. Solid-State Electrochemical Kinetics of Li-Ion Intercalation into $Li_{1-x}CoO_2$: Simultaneous Application of Electroanalytical Techniques Sscv, Pitt, and Eis. *J. Electrochem. Soc.* **1998**, *146*, 1279−1289.
(38) Mohamedi, M.; Takahashi, D.; Uchiyama, T.; Itoh, T.; Nishizawa, M.; Uchida, I. Explicit Analysis of Impedance Spectra Related to Thin Films of Spinel $LiMn_2O_4$. *J. Power Sources* **2001**, *93*, 93−103.
(39) Zhang, S. S.; Xu, K.; Jow, T. R. Eis Study on the Formation of Solid Electrolyte Interface in Li-Ion Battery. *Electrochim. Acta* **2006**, *51*, 1636−1640.
(40) Ramana, C. V.; Massot, M.; Julien, C. M. Xps and Raman Spectroscopic Characterization of $LiMn_2O_4$ Spinels. *Surf. Interface Anal.* **2005**, *37*, 412−416.
(41) Shaju, K. M.; Subba Rao, G. V.; Chowdari, B. V. R. Lithiated O_2 Phase, $Li_{(2/3)+X}(Co_{0.15}Mn_{0.85})O_2$ as Cathode for Li-Ion Batteries. *Solid State Ionics* **2002**, *152*−*153*, 69−81.

DOI: 10.1021/acs.jpcc.5b10298
J. Phys. Chem. C 2015, 119, 28776−28782